

Published in final edited form as:

Nat Commun. ; 3: 818. doi:10.1038/ncomms1826.

Hydroxylation of 5-methylcytosine by TET2 maintains the active state of the mammalian *HOXA* cluster

Michael T. Bocker¹, Francesca Tuorto^{1,2}, Günter Raddatz¹, Tanja Musch¹, Feng-Chun Yang³, Mingjiang Xu³, Frank Lyko¹, and Achim Breiling¹

¹Division of Epigenetics, DKFZ-ZMBH Alliance, German Cancer Research Center, Im Neuenheimer Feld 580, 69120 Heidelberg, Germany

²Institute of Genetics and Biophysics ABT, CNR, Via Pietro Castellino 111, 80131 Naples, Italy

³Herman B Wells Center for Pediatric Research, Indiana University Melvin and Bren Simon Cancer Center, Indiana University School of Medicine, 1044 W. Walnut Street, Indianapolis, IN 46202, United States

Abstract

Differentiation is accompanied by extensive epigenomic reprogramming, leading to the repression of stemness factors and the transcriptional maintenance of activated lineage-specific genes. Here we use the mammalian *Hoxa* cluster of developmental genes as a model system to follow changes in DNA modification patterns during retinoic acid induced differentiation. We find the inactive cluster to be marked by defined patterns of 5-methylcytosine (5mC). Upon the induction of differentiation, the active anterior part of the cluster becomes increasingly enriched in 5-hydroxymethylcytosine (5hmC), following closely the colinear activation pattern of the gene array, which is paralleled by the reduction of 5mC. Depletion of the 5hmC generating dioxygenase Tet2 impairs the maintenance of *Hoxa* activity and partially restores 5mC levels. Our results indicate that gene specific 5mC-5hmC conversion by Tet2 is crucial for the maintenance of active chromatin states at lineage-specific loci.

Keywords

DNA methylation; *Hoxa* cluster; 5-hydroxymethylcytosine; epigenetic maintenance; Ten-Eleven-Translocation 2 (Tet2)

Introduction

In the developing mammalian embryo the characteristic features of the body plan are defined by the coordinated expression of homeotic (*Hox*) genes in an anterior-posterior order. *Hox* genes show a clustered organization where the arrangement of transcription units on the chromosome often mirrors their spatiotemporal expression domains along the anterior-posterior axis of the developing embryo^{1,2}. These particular patterns of transcription

Correspondence should be addressed to: Achim Breiling, German Cancer Research Center, Division of Epigenetics, Im Neuenheimer Feld 580, 69120 Heidelberg, Germany, Phone: +49-6221-423804, Fax: +49-6221-423802, a.breiling@dkfz.de.

Author contribution

AB and FL conceived the study. MB, FL and AB designed the experiments and interpreted results. FCY and MX provided mouse tissues. MB, FT, TM and AB performed the experiments. MB and GR performed the bioinformatic analyses. MB, FL and AB wrote the manuscript.

Conflict of interest

The authors declare that they have no conflict of interest.

are usually induced and regulated by morphogens, like all-trans-retinoic acid (RA), a conserved intercellular signaling molecule found in most vertebrates³. In pluripotent cell populations *Hox* genes are tightly repressed, but kept in a poised chromatin state that allows rapid lineage-specific expression upon morphogen induction⁴.

A prominent example of a poised developmental gene array is the *Hoxa* cluster. In stem cells, this cluster is silenced by repressive complexes of the Polycomb group (PcG) and characterised by the presence of bivalent histone methylation marks⁵. *Hoxa* activation has been extensively studied in cell culture, using embryonic stem cells (ESCs) or embryonal carcinoma (EC) cell lines^{6,7}. In these systems, RA treatment induces colinear derepression of the anterior *Hoxa* genes, which is accompanied by the progressive loss of PcG proteins and repressive histone modifications^{8–10}. Despite the presence of several CpG islands within the cluster, the role of DNA methylation in *Hoxa* regulation is poorly understood. The inactive *Hoxa* cluster was found strongly methylated in differentiated fibroblasts and monocytes, but also in cancer cell lines and tumours^{11–13}. Nevertheless, there are also regions with significant DNA methylation throughout the cluster in undifferentiated stem cells or embryonal carcinoma cells, often coinciding with promoter regions or regulatory elements^{13,14}.

The presence of 5-methylcytosine (5mC) at or near promoter regions of genes is thought to be mostly incompatible with activated transcription, indicating that methylated cytosines have to be removed or converted to ensure the maintenance of the active state^{15,16}. The recent mapping of 5-hydroxymethylcytosine (5hmC) in the mouse genome shed light on a potential demethylation pathway that is triggered by the conversion of 5-methylcytosine to 5-hydroxymethylcytosine^{17,18}. Additional processing steps and base-excision repair mechanisms would then result in the removal of the methylated base and its substitution with an unmethylated cytosine¹⁸. 5hmC is generated from existing 5mC by the ten-eleven translocation (TET) family of proteins^{19,20}. Two of these enzymes, *Tet1* and *Tet2*, are significantly expressed in mouse ESCs²⁰. Their depletion has been shown to lead to a partial loss of the undifferentiated state and to induce differentiation towards trophoectodermal, endodermal and mesodermal lineages^{19–21}. This suggests that both proteins have an important role in maintaining pluripotency by controlling 5hmC levels and thus orchestrate the balance between stemness and lineage commitment^{20, 21}.

In mouse embryonic stem cells 5hmC has been mostly associated with euchromatin, gene bodies and active genes^{21,22}, suggesting that the presence of 5hmC facilitates activated transcription. Nevertheless, 5hmC and *Tet1* were also found enriched in or near inactive genes with bivalent chromatin marks^{23–25}. Here, 5hmC could prime for rapid activation, either by triggering DNA demethylation or by recruiting transcriptional regulators that recognise 5hmC²³. Taken together, 5mC-5hmC conversion seems to protect active genes and poised bivalent domains from becoming permanently methylated and might be needed for fine-tuning regulated transcription and for protecting the genome from unspecific DNA methylation^{23,24}.

Importantly, however, the presence of 5hmC is not restricted to embryonic stem cells. *Tet2* is expressed in a variety of differentiated tissues, especially in the haematopoietic and neuronal lineages, in brain, neuronal progenitors and postmitotic neurons^{19,26–28}. Furthermore, *Tet2* mutations are frequent in patients with myeloid leukaemias, a group of diseases that is characterised by impaired differentiation of myeloid precursor cells^{29,30}. Nevertheless, the functional role of cytosine hydroxymethylation during differentiation has remained unclear.

In order to study 5mC and 5hmC levels in relation to activated transcription in a defined genomic region we focused on the human *HOXA* cluster and followed DNA methylation patterns in the pluripotent human embryonic carcinoma cell line NTERA2 D1 during RA-induced differentiation. We found that CpG-rich regions in the anterior part of the cluster showed significant 5mC-5hmC conversion during RA-induced *HOXA* activation that followed the colinear gene expression pattern in NT2 cells. Small interfering RNA-mediated depletion of TET2 during RA induction impaired the maintenance of *HOXA* activity and partially restored genomic 5mC levels. Tissue-specific *Hoxa* gene expression patterns were also significantly reduced in a *Tet2* knock out mouse model, suggesting a general role of Tet2 for the maintenance of active expression patterns in the cluster. These results indicate that Tet2-dependent conversion of repressive 5mC to 5hmC is crucial for the maintenance of open chromatin states and active gene expression patterns.

Results

A human embryonic carcinoma cell line as stem cell model

The embryonal carcinoma cell line NTERA2 D1 (NT2) represents a well-established model system to study *HOX* cluster regulation⁶. NT2 cells have not only been shown to differentiate along the neuronal lineage upon RA induction, but also show mesodermal and ectodermal lineage potential and are thus considered to be a valuable stem cell model system^{31,32}. They express high levels of the stem cell specific transcription factor OCT4, other stemness factors, PcG proteins and DNA methyltransferases (Fig. 1a; ref. 14). Expression of pluripotency genes and the DNA methyltransferase DNMT3B is rapidly reduced upon RA-dependent differentiation (Fig. 1a, 1b).

In order to study detailed DNA methylation patterns before and after RA induction, we analysed genomic DNA of RA-treated and untreated NT2 cells using Infinium450K BeadChips (Illumina). These arrays interrogate more than 450,000 methylation sites in the human genome, including CpG islands (CGIs), CpG sites outside of CGIs and non-CpG methylation sites identified in human embryonic stem cells³³. Low levels of strand specific DNA methylation outside the CpG context have been found specifically in mouse and human embryonic stem cells^{34,35}. Interestingly, NT2 cells also showed significant levels of non-CpG methylation that was greatly reduced upon RA-induced differentiation (Fig. 1c), which further illustrates the value of this cell line as a human stem cell model.

DNA methylation analysis in differentiating NT2 cells

A detailed analysis of the Infinium450K data showed significant dynamic changes in site-specific genomic methylation patterns, which increased during RA treatment (Fig. 1d). After 14 days of RA induction, 2629 individual markers were hypomethylated and 1225 markers hypermethylated compared to the untreated control, which corresponds to 1286 differentiation-dependent hypomethylated and 529 hypermethylated genes. Array-predicted methylation changes were experimentally validated by 454 bisulfite sequencing (see below) and thus represent genuine epigenetic changes associated with RA-induced differentiation.

Further data analysis addressed the molecular characteristics of differentially methylated sites. Hypomethylated sites were substantially less frequently associated with CGIs (including annotated shelf and shore regions) when compared to hypermethylated sites or to all sites represented on the array (Fig. 1e). Interestingly, differentially methylated sites were more frequently associated with CpG island shores, which is in line with previous reports showing that the majority of DNA methylation variation occurs in shores rather than in CGIs³⁶. Additional characterization showed that differentially methylated sites were significantly associated with enhancer regions (Fig. 1f). Pathway analyses of differentially

methylated genes revealed ‘gene expression’ and ‘cellular development’ as the most significantly enriched molecular and cellular functions (Supplementary Figure S1). Furthermore, the most significantly enriched physiological function identified for the hypomethylated gene set was ‘nervous system development and function’ (Supplementary Figure S1), suggesting that DNA methylation plays a role in the neuronal differentiation induced by RA treatment of NT2 cells.

Epigenetic changes in the activated *HOXA* cluster

One of the best-studied genomic regions in NT2 cells is the anterior half of the *HOXA* cluster, which is colinearly activated upon RA treatment (Fig. 2a; refs. 8 and 9). *HOXA1* was rapidly activated, and peaked after 3 days of RA treatment, whereas *HOXA2* and *HOXA3* levels were steadily increasing over the course of the experiment. Expression of *HOXA4* and *HOXA5* started to increase after 3 days of RA exposure, whereas *HOXA6* only began to be expressed after 14 days. The posterior part of the cluster, starting with *HOXA7*, does not respond to RA in NT2 cells^{8,9}.

HOXA activation is accompanied by rapid changes of histone modification patterns^{8,9}. We followed epigenetic changes in the *HOXA1* region by chromatin immunoprecipitation (X-ChIP) using antibodies against modified variants of histone H3. As expected, the *HOXA1* promoter was marked by bivalent chromatin (trimethylation of lysine 4 and 27) in the uninduced state (Supplementary Figure S2). Upon RA treatment, these structures were resolved to H3K4me3 and H3K27me3 was successively lost (Supplementary Figure S2). In contrast, an exonic *HOXA1* region, containing one of the few potential NANOG/OCT4 binding sites in the cluster³⁷, was mainly marked by H3K27me3 in the uninduced state. Upon RA treatment, this pattern rapidly changed to H3K4me3, which reflects the activated transcription of the gene (Supplementary Figure S2).

The *HOXA* cluster is characterised by several CpG-rich regions that often localise near transcription units, suggesting the involvement of DNA methylation in their regulation⁹. We therefore extracted the 383 CpG sites associated with the cluster from the Infinium450K data and analysed their methylation status (Fig. 2b and 2c). Many of these sites were methylated in untreated NT2 cells, especially downstream of *HOXA1*, in the gene body of *HOXA3*, between *HOXA5* and *HOXA7* and also in the *HOXA9* gene body (Fig. 2c). This pattern did not change significantly upon RA treatment for 14 days, which is in contrast to the strong activation of the anterior part of the cluster observed during this time period (Fig. 2a and 2c). We validated and expanded this analysis using deep 454 bisulfite sequencing of selected CpG-rich regions of the cluster after 3 weeks of RA treatment (Fig. 2d). We obtained very similar results, with highly methylated regions downstream of *HOXA1*, in the *HOXA3* gene body, in several regions between *HOXA4* and *HOXA7* and in the *HOXA9* locus. Similar patterns were also described in human ESCs using high throughput bisulfite sequencing¹³. Again, most of these regions did not change their methylation state upon differentiation, even after 3 weeks (Fig. 2d). A notable exception was the first exon of *HOXA1* that showed significant demethylation after 14 days of RA treatment (Fig. 2c), which was further increased after 21 days (Fig. 2d). We have previously shown that a knock down of the maintenance DNA methyltransferase DNMT1 leads to a significant loss of DNA methylation in CpG islands of the *HOXA* cluster¹⁴. We thus measured the expression levels of the first three *HOXA* genes after three days of DNMT1 depletion and found a significant but weak derepression of these genes (Supplementary Figure S3). Nevertheless, this effect was minimal compared to RA induction, indicating that DNA methylation might have an accessory role in *HOXA* repression.

Increased 5-hydroxymethylation in the activated *HOXA* cluster

The persistence of DNA methylation patterns in RA-induced cells appeared to contradict the colinear transcriptional activation of the *HOXA* cluster, which is accompanied by clear epigenetic changes on the level of histone modifications (Supplementary Figure S2; refs. 8 and 9). However, our methods for DNA methylation analysis were based on bisulfite conversion, which does not distinguish between 5-methylcytosine and 5-hydroxymethylcytosine³⁸. If *HOXA* activation was accompanied by oxidation of 5mC to 5hmC, this conversion could not have been detected by our methods. We therefore used methylated DNA immunoprecipitation with specific antibodies^{21,22} against 5mC (MeDIP) and 5hmC (hMeDIP) and massive parallel sequencing to examine changes in 5mC and 5hmC distribution during RA-induced differentiation of NT2 cells. We obtained 10 to 50 million reads for each sample (Supplementary Table S1), which were mapped to the most recent human genome assembly (GRCh37/hg19). All reads from the cluster were extracted and read coverage over genomic *HOXA* regions were calculated. As shown in Figure 3a we found high levels of DNA methylation at specific regions in untreated NT2 cells, often related to CpG islands, which closely correspond to our Infinium450K and 454 bisulfite sequencing results. Interestingly, 5mC was basically absent at potential retinoic acid response elements (RAREs) of the anterior cluster⁹, which might indicate their accessibility (Fig. 3a). 5-hydroxymethylation was found to be evenly distributed at low levels throughout the cluster in untreated NT2 cells. Upon RA treatment, a strong overall increase in 5hmC levels was observed in the activated part of the cluster (*HOXA1-HOXA6*). This is shown in more detail for the *HOXA1* region in Figure 3b. Of note, we also observed that increasing levels of 5hmC were paralleled by a reduction of 5mC, in particular in the *HOXA1* region (Fig. 3b).

In order to validate the sequencing data and to extend the time frame of the analysis, we repeated the immunoprecipitation analysis with genomic DNA from untreated NT2 cells and cells treated for 3, 7, 14 and 21 days with RA and analysed the immunopurified DNA by gene specific real-time-PCR at selected genomic regions (see Fig. 3 for amplicon positions). The human genes *UEB2B* and *HIST1H3B* served as unmethylated control regions (Supplementary Figure S4). As shown in Figure 4, the (h)MeDIP-seq data was essentially confirmed. We found high levels of 5mC at the CpG island downstream of *HOXA1*, at exonic regions of *HOXA1*, *HOXA3*, *HOXA4*, an intergenic region between *HOXA5* and *6* and at the *HOXA6* promoter. Lower, but significant levels of DNA methylation were also present at the promoters of *HOXA1* and *HOXA2*. Except for the CpG island downstream of *HOXA1*, we also detected low levels of DNA hydroxymethylation in all these regions (Fig. 4). Hydroxymethylation significantly increased during RA treatment, which was accompanied by decreasing 5mC levels (Fig. 4). Taken together, our results show that during RA-induced differentiation, the anterior part of the *HOXA* cluster loses 5-methylcytosine marks and gains significant levels of 5-hydroxymethylcytosine. These changes follow the physiological colinear activation pattern of the cluster: changes were greater for anterior genes that respond faster and stronger to RA (*HOXA1*, *HOXA2*) than for posterior genes that respond slower (*HOXA5*, *HOXA6*). In addition, after 21 days of RA treatment, we also observed a low degree of total (5hmC plus 5mC) demethylation, especially for the promoters of *HOXA1* and *HOXA2* and the second exon of *HOXA4*. This finding probably reflects further oxidation of hydroxymethylated cytosines after prolonged RA treatment.

TET2 mediates hydroxymethylation in the *HOXA* cluster

To address mechanistic aspects behind the observed methylation changes, we analysed the expression of *TET1-3* in differentiating NT2 cells. As shown in Figure 5a, *TET1* was highly expressed in uninduced NT2 cells, consistent with the pluripotent potential of the cell line.

TET2 and *TET3* were expressed at much lower levels. Upon RA induction, *TET1* was downregulated, whereas *TET2* and *TET3* were significantly upregulated (Fig. 5a). In order to analyze the role of TET proteins in maintaining the active state of the *HOXA* cluster, NT2 cells were treated with RA for 3 days, followed by siRNA-mediated knock down of TET enzymes. Quantitative RT-PCR analysis of *TET1–3* mRNA levels showed that the depletion was effective (Fig. 5b) and comparable to other publications²¹. The expression of the most proximal *HOXA* genes, especially of *HOXA1* and *HOXA2*, was significantly lower for the *TET2* knock down when compared to the control (Fig. 5c). Also, *HOXA3*, *HOXA4* and *HOXA5* were less expressed upon knock down of *TET2*. A combination of *TET1* and *TET2* knock down, that was shown to have the strongest effect on the derepression of pluripotency-related genes in mouse ESCs²¹, gave similar results (Fig. 5c).

Next we investigated the functional role of TET proteins for the methylation state of the cluster. Again NT2 cells were treated for 3 days with RA, followed by knock down of TET enzymes. Genomic DNA was then prepared and analysed by (h)MeDIP, with a focus on the four *HOXA*-regions that showed significant methylation changes upon RA treatment: the promoters of *HOXA1* and *HOXA2*, a CpG-rich region of *HOXA3* and the second exon of *HOXA4*. As shown in Figure 6, the patterns observed for the control are in excellent agreement with the (h)MeDIP-seq data shown in Figure 4. Knock down of *TET1* and *TET3* did not change these patterns, whereas *TET2* depletion led to reduced levels of 5hmC in all four regions, while 5mC levels became partially restored. An even stronger effect was observed when *TET1* and *TET2* were simultaneously depleted, leading to 5mC levels that approached untreated NT2 cells (Fig. 6). Thus, *TET2* depletion reverses the epigenetic DNA methylation changes induced by retinoic acid, which results in defects in the maintenance of the active state of the *HOXA* cluster.

Knock out of Tet2 leads to reduced Hoxa expression

Finally, in order to further confirm a role for Tet2 in *Hoxa* transcriptional maintenance, we also measured *Hoxa* expression levels in various mouse tissues and compared them to *Tet2* knock out tissues³⁹. Total RNA of samples of an one year old *Tet2*^{-/-} mouse and a wild type animal with the same genetic background was prepared and *Hoxa* and *Tet* expression patterns were analysed (Fig. 7). We restricted further analysis to seven tissues that were previously reported to contain significant 5hmC levels^{26–28} and showed clear *Tet2* and *Hoxa* expression patterns in adult wild type mice (Fig. 7a). With very few exceptions, active *Hoxa* genes showed significantly reduced expression levels in the corresponding *Tet2*^{-/-} tissues (Fig. 7b-e; Supplementary Figure S5). In contrast, *Tet1* and *Tet3* patterns remained mostly unchanged. Finally, to analyse the effect of the *Tet2* deletion on the methylation state of the murine *Hoxa* cluster, we performed (h)MeDIP using wild type and *Tet2*^{-/-} genomic DNA of three tissues that showed significant *Hoxa* expression patterns in wild type mice (kidney, spleen, lung). We restricted our analysis to four genomic fragments, corresponding to regions that contain the promoter or reside in the first exon of *Hoxa2*, *Hoxa4*, *Hoxa5* and *Hoxa7*, respectively (Fig. 8a). The results showed that loss of *Tet2* induced a significant increase of 5mC in these regions, paralleled by a reduction of 5hmC (Fig. 8b–e). These changes are in excellent agreement with the reduced expression levels observed for these genes in these tissues (Fig. 7c–e). These data confirm a general role for Tet2 in controlling 5hmC levels and thereby the maintenance of active expression patterns in the mammalian *Hoxa* cluster.

Discussion

In this study we show that the repressed human *HOXA* cluster is characterised by a specific pattern of 5-methylcytosine and 5-hydroxymethylcytosine marks. Both marks appeared to decorate larger regions, similar to the domains described for bivalent histone modifications

in repressed *HOX* clusters⁵. Upon differentiation, the anterior half of the cluster became active and was marked by high levels of 5hmC. In parallel, 5mC levels were reduced, especially in the *HOXA1* and *HOXA2* regions. A more detailed analysis of selected *HOXA*-loci revealed that the increase of 5hmC followed the colinear gene activation pattern of the cluster, i.e. expression changes and higher 5hmC levels were first observed at proximal *HOXA* genes, whereas more distal genes showed delayed activation and responded substantially later. These findings further underscore the association of the 5hmC mark with activated *HOXA* transcription.

We identified TET2 as an important factor for the RA-induced 5mC-5hmC conversion. *TET2* was significantly upregulated in RA-treated NT2 cells. Knock down of TET2 after 3 days of RA treatment led to a significant decrease in expression levels of the anterior *HOXA* genes, indicating that the maintenance of their transcription is disturbed. This appeared to be directly caused by reduced hydroxymethylation, as TET2 knock down also led to reduced 5hmC levels at selected *HOXA* regions and partially restored 5mC levels. Our data suggest that the 5mC-5hmC conversion by TET2 at neuronal selector genes (like the anterior *HOXA* cluster), is important for ongoing differentiation processes that depend on their expression. A comparable role for Tet2 has been suggested for the haematopoietic lineage. *Tet2* is highly expressed in erythroid precursors and granulocytes²⁹ and loss of the protein has been shown to lead to various haematopoietic differentiation defects^{39,40-42}.

Furthermore, our results obtained with tissues from *Tet2*^{-/-} mice³⁹ suggest that *Hoxa* expression patterns in terminally differentiated tissues are also negatively affected by the deletion of *Tet2*. Interestingly, the tissues that showed the strongest effect were kidney, lung and the spleen, which also showed the highest Tet2 expression levels. These tissues showed a clear reduction of 5hmC in *Hoxa* target regions in the *Tet2*^{-/-} mouse and significantly increased 5mC levels, which corresponded to the reduced *Hoxa* transcription. Nevertheless, *Hoxa* genes remained active at lower levels, which might explain the lack of strong developmental phenotypes in *Tet2*^{-/-} mice. As shown in our knock down experiments in NT2 cells, a partial redundancy between TET1 and TET2 cannot be excluded, and it will be interesting to analyze the developmental phenotypes of *Tet1*^{-/-}/*Tet2*^{-/-} double mutant mice.

Interestingly, the specific patterns of *HOXA* methylation we have identified in untreated NT2 cells did not prevent initial transcriptional activation. For the first three *HOXA* genes high transcriptional activity can be observed already after a few hours of RA treatment⁹, when methylation patterns have not yet changed. *HOXA* activation during development strongly depends on the interaction of the ligand-bound retinoic acid receptors with specific RAREs, the subsequent changes in histone modifications and the recruitment of activating protein complexes^{10,43}. In agreement with this notion, we found that reduction of DNA methylation by depletion of DNMT1 only led to a minimal *HOXA* activation in untreated NT2 cells. It is known that the repressed cluster has a particular higher order structure and that transcriptional activation is accompanied by structural changes within the cluster^{10,44,45}. Changes in DNA methylation patterns during differentiation might thus influence the three-dimensional architecture of the cluster and thus affect the maintenance and fine-tuning of gene expression states⁴⁶. Our data indicate that once the cluster has been activated, 5mC-5hmC conversion is necessary for the maintenance of RA-induced transcription patterns and active higher order structures.

While most regions with RA-induced 5hmC show already significant cytosine methylation in untreated NT2 cells, we also observed elevated 5hmC levels in some regions (mostly outside of CpG islands) that appeared not to be marked by 5mC. It should be noted that the 5mC antibody used in our experiments is significantly less efficient in dot blots and in immunoprecipitations, when compared to the 5hmC antibody²¹⁻²³. In addition, its binding

depends much more on the CpG density in the DNA fragments²³. Thus, in regions with low CpG density, 5mC will not be recognised very well (or not at all), whereas detection of 5hmC will be more efficient. Nevertheless, our Infinium450K data show that total DNA methylation levels in the *HOXA* cluster did not change significantly upon RA treatment for 14 days for most of the interrogated sites (Fig. 3a, bottom panel). This indicates that 5hmC signals detected after RA treatment largely depend on pre-existing 5mC.

Although we could observe some degree of total DNA demethylation after prolonged RA treatment in NT2 cells, the overall rate appeared rather low. While we did not analyse further processing and excision of the 5hmC mark in later stages, the substantial levels of 5hmC during the first three weeks of differentiation and the colinear pattern of 5mC-5hmC conversion indicate that already the presence of 5hmC allows the maintenance of active higher order structures. Interestingly, it was shown that oxidation of cytosines in CpG-rich regions reduces significantly the binding of methyl-CpG binding proteins and DNA methyl transferases^{47,48}. Thus 5mC-5hmC conversion might passively inhibit the maintenance of repressive structures by disturbing DNA-protein interactions. In addition, chromatin remodeling complexes can directly interact with regions marked with 5hmC and influence 5hmC patterns⁴⁹, which suggests that 5hmC itself can be read as an epigenetic mark. The three mouse tissues we used for (h)MeDIP analysis, despite high expression of *Tet2*, harbour very different total 5hmC levels^{26–28,39,40}. Our results show that knock out of *Tet2* results in a general strong increase of 5mC in these tissues. This suggests tissue specific differences regarding the further processing of 5hmC, which is in line with recent findings that tissue type is the major determinant of 5hmC content⁵⁰.

In conclusion, we envisage the repressed *HOXA* cluster to be marked by specific methylation patterns and to be part of a silent looped structure in pluripotent cells. After RA induction activated genes would move sequentially or by specific looping interactions to an open compartment (Supplementary Figure S6). This is accompanied by progressive 5-hydroxymethylation, which prevents DNA re-methylation and gene re-silencing.

Material and Methods

Cell culture

The human cell line NT2 D1 was a kind gift from Peter W. Andrews. Cell line authentication was provided by LGC Standards (Teddington, report tracking no. 71008933). NT2 cells were maintained in Dulbecco's Modified Eagle Medium (D-MEM, with l-glutamine, 4500 mg/l d-glucose, without sodium pyruvate; Gibco) supplemented with 10% fetal bovine serum and 200 U/ml penicillin and 200 µg/ml streptomycin (all from Gibco) in a humidified atmosphere of 5% CO₂ in air. NT2 cells were induced to differentiate with 10 µM all-trans retinoic acid (Sigma). Medium containing RA was changed every 2 days. Cells were harvested by trypsin treatment and stored at –80 °C.

Protein depletion via siRNAs

For depletion of TET1, TET2, TET3 and DNMT1 ON-TARGETplus SMARTpool siRNAs (Dharmacon) were used. Untreated NT2 cells or cells treated for 3 days with RA were seeded into 6-well plates at a density of 2×10^5 in 2 ml of medium. siRNAs were transfected with the DharmaFECT1 transfection reagent (Dharmacon). The final siRNA concentration was 50 nM. Cells were harvested after 72 hours and pellets were stored at –80°C. Scrambled siRNAs for negative control experiments (non-targeting pool) were also obtained from Dharmacon.

RT PCR and real time analysis

Total RNA from RA-induced and untreated NT2 cells was prepared using the Trizol reagent (Invitrogen). Real-time RT-PCR was performed using the QuantiTect Reverse Transcription Kit (Qiagen). One μg of total RNA was processed in 20 μl reactions. One μl of cDNA was used for a 10 μl PCR reaction using the Absolute QPCR SYBR Green Mix (Thermo Scientific) and a Roche LightCycler 480. PCR conditions: 1 cycle: 95°C×15 minutes; 50 cycles: 95°C×15 seconds, 60°C×40 seconds, read; melting curve 65°C–95°C, read every 1°C. Cycle threshold numbers for each amplification were measured with the LightCycler 480 software and relative expression values were calculated and normalised using *β -actin* and *lamin-b* as internal standards. qRT-PCR measurements were repeated at least three times on biological replicates. For primer sequences see Supplementary Table S2.

Array based DNA methylation profiling and data analysis

Genomic DNA from RA-induced and untreated NT2 cells was prepared using the DNeasy Blood & Tissue Kit (Invitrogen). Array-based gene-specific DNA methylation analysis was performed using Infinium HumanMethylation450 bead chip technology (Illumina, San Diego, CA, USA). Genomic DNA (500 ng) from each sample was bisulfite converted using the EZ-96 DNA Methylation Kit (Zymo Research Corporation). Bisulfite treated genomic DNA was whole-genome amplified and hybridised to HumanMethylation450 BeadChips. The methylation status of a specific cytosine was indicated by average beta (AVB) values where 1 corresponds to full methylation and 0 to no methylation. Raw array data were quantile normalised and p-values for comparisons between different datasets were statistically adjusted using the Benjamini-Hochberg correction as described previously⁵¹. Individual loci were scored as differentially methylated if the AVB difference was greater than or equal to 0.2. Functional categories of differentially methylated genes were identified by Ingenuity Pathway Analysis (www.ingenuity.com). The Infinium methylation data is available at the Gene Expression Omnibus (GEO) at the National Center for Biotechnology Information (NCBI) under accession code GSE33130.

454 DNA bisulfite sequencing

Deep DNA bisulfite sequencing was performed as described previously⁵¹. For 454 sequencing, bisulfite-treated genomic DNA was amplified using sequence-specific primers containing cell type-specific barcodes and 454 linker sequences (see Supplementary Table S3).

ChIP assay

Crosslinked chromatin from untreated or RA-treated NT2 cells was prepared and immunoprecipitated as described previously¹⁴. ChIP-grade antibodies specific for H3K27me3 (07-449) and H3K4me3 (07-473) were purchased from Upstate. Immunoprecipitates were finally dissolved in 30 μl of TE buffer (10 mM Tris-HCL pH 8, 1 mM EDTA). One μl was analysed by real time PCR using *HOXA1*-specific primer pairs (see Supplementary Table S4) in 10 μl PCR reactions, using the Absolute QPCR SYBR Green Mix (Thermo Scientific) and a Roche LightCycler 480. PCR conditions: 1 cycle: 95°C×15 minutes; 50 cycles: 95°C×15 seconds/60°C×40 seconds, read; melting curve 65°C–95°C, read every 1°C. Cycle threshold numbers for each amplification were measured with the LightCycler 480 software and enrichments were calculated as percentage of the input.

MeDIP and hMeDIP

Methylated DNA immunoprecipitation was performed as described⁵². Genomic DNA from NT2 cells or mouse tissues was randomly sheared using a Bioruptor (Diagenode). 5 μg of

sonicated DNA was used for immunoprecipitations with 2 µg of antibodies specific for 5-methylcytosine (monoclonal; Active Motif, 39649) and 5-hydroxymethylcytosine (polyclonal, Active Motif, 39791). Co-precipitated DNA was finally resolved in 60 µl TE buffer. Two µl of the IP or 20 ng of input DNA were analysed by real time PCR using specific primer pairs (see Supplementary Table S4) in 10 µl PCR reactions, using the Absolute QPCR SYBR Green Mix (Thermo Scientific) and a Roche LightCycler 480. PCR conditions: 1 cycle: 95°C×15 minutes; 50 cycles: 95°C×15 seconds/60°C×40 seconds, read; melting curve 65°C–95°C, read every 1°C. Cycle threshold numbers for each amplification were measured with the LightCycler 480 software and enrichments were calculated as percentage of the input. As negative controls for unmethylated regions served *UEB2B* and *HIST1H3B* for human samples or the *mGapdh* and *mBeta-actin* promoters for mouse⁵² (Supplementary Figure S4). Final enrichments were calculated relative to these unmethylated controls as described⁵². For primer sequences see Supplementary Table S4.

(h)MeDIPs-Seq

Genomic DNA was purified from untreated and RA-treated NT2 cells as described above. Fifty µg of genomic DNA for each sample was sonicated to 300bp fragments using a Covaris S220 (Covaris). Sheared DNA was ethanol precipitated, washed with 70% ethanol, and dissolved in TE buffer (pH8.0). Illumina adapters were ligated as described²⁵ using the End-It DNA End-repair kit (Epicentre). DNA was purified with the QiaQuick PCR purification kit (Qiagen) and diluted to 122.5µl with ddH₂O. After the addition of 15µl NEB buffer 2, 3.5µl of 10mM ATP and 9µl of 5U/µl Klenow *exo*⁻ (NEB), reactions were incubated at 37°C for 50min. DNA was subsequently purified with the QiaQuick PCR purification kit, diluted to 24µl with ddH₂O, and mixed with 50µl of 2x NEB quick ligation buffer, 20 µl of barcoded Illumina adapter and 6µl of quick T4 DNA ligase (NEB). After 20 minutes incubation at room temperature, DNA was purified again with QiaQuick PCR purification kit. Ligation efficiency was analyzed by PCR on 10ng of final ligated DNA with Illumina sequencing primers. Finally, five µg of adapter ligated DNA was used for the immunoprecipitation, as described above. Immunoprecipitated DNA was resolved in 20µl of water and all (h)MeDIP samples were pooled to create the MeDIP and hMeDIP libraries, respectively. Both libraries were purified on e-Gel (Invitrogen) and the 300bp bands (containing roughly 200bp fragments of adapter-ligated immunopurified DNA) were extracted. Libraries were amplified using Illumina-Enrichment Primers for 12 cycles and purified using Agencourt AMPure XP beads (Beckman Coulter). DNA concentrations were measured using a Agilent High Sensitivity DNA Assay (Agilent Technologies) and 7 pmol were used for cluster PCR and substantial 50bp single-end sequencing on a HiSeq2000 (Illumina).

Mapping of sequencing data

All processing steps of the sequencing data were carried out using the short read analysis pipeline shore⁵³. Reads were trimmed by removing stretches of bases having a quality score <30 at the ends of the reads. The trimmed reads were mapped to the most recent human genome assembly hg19 using the mapping program bowtie⁵⁴. After the mapping duplicate reads were removed and the position-wise coverage of the *HOXA* cluster by sequencing reads was integrated as custom tracks in the UCSC genome browser⁵⁵ (<http://genome.ucsc.edu/>). The sequencing data is available at Gene Expression Omnibus (GEO) under accession code GSE33130.

Gene expression analysis in *Tet2* knockout mice

Tet2 knock out mice have been described previously³⁹. One female *Tet2*^{-/-} mouse and one wild type female of the same genetic background were sacrificed and 18 tissue samples (total brain, heart, kidney, spleen, liver, pad, chest bone, nose, tongue, tail, skin, eye, small

intestine, skeletal muscle, spinal chord, uterus, ovary and lung) were taken and immediately frozen in liquid nitrogen for storage at -80°C . Total RNA was prepared using the Trizol reagent (Invitrogen) and a TissueRuptor (Qiagen). Real-time RT-PCR was performed as described above. Relative quantifications of expression status of the genes under observation comparing treated to non-treated cells were calculated and normalised using mouse β -actin and *GPDH* as internal standards. qRT-PCR measurements were repeated at least three times on technical replicates. For mouse-specific primer sequences see Supplementary Table S2. All mouse studies were approved by the MSSM Animal Care and Use Committee.

Supplementary Material

Refer to Web version on PubMed Central for supplementary material.

Acknowledgments

We thank Peter W. Andrews (University of Sheffield) for the original NT2 cells, Kristian Helin (University of Copenhagen) for human *HOXA*-specific RT-primer sequences, Janetta Bijl (Hôpital Maisonneuve-Rosemont, Montreal) for murine *HOXA*-specific RT-primer sequences and Rudolf Jaenisch (Whitehead Institute for Biomedical Research, Cambridge) for advice on *Tet2* mutant mice. This work was supported by grants from the Deutsche Forschungsgemeinschaft (Priority Programmes 1356 and 1463) to AB and FL. We are particularly thankful to André Leischwitz and the DKFZ Genomics and Proteomics core facility for high throughput sequencing and overall support.

References

- Duboule D, Morata G. Colinearity and functional hierarchy among genes of the homeotic complexes. *Trends Genet.* 1994; 10:358–364. [PubMed: 7985240]
- Kmita M, Duboule D. Organizing axes in time and space; 25 years of colinear tinkering. *Science.* 2003; 301:331–333. [PubMed: 12869751]
- Duester G. Retinoic acid synthesis and signaling during early organogenesis. *Cell.* 2008; 134:921–931. [PubMed: 18805086]
- Soshnikova N, Duboule D. Epigenetic regulation of Hox gene activation: the waltz of methyls. *Bioessays.* 2008; 30:199–202. [PubMed: 18293357]
- Bernstein BE, et al. A bivalent chromatin structure marks key developmental genes in embryonic stem cells. *Cell.* 2006; 125:315–326. [PubMed: 16630819]
- Boncinelli E, Simeone A, Acampora D, Mavilio F. HOX gene activation by retinoic acid. *Trends Genet.* 1991; 7:329–334. [PubMed: 1685814]
- Langston AW, Gudas LJ. Retinoic acid and homeobox gene regulation. *Curr Opin Genet Dev.* 1994; 4:550–555. [PubMed: 7950323]
- Bracken AP, Dietrich N, Pasini D, Hansen KH, Helin K. Genome-wide mapping of Polycomb target genes unravels their roles in cell fate transitions. *Genes Dev.* 2006; 20:1123–1136. [PubMed: 16618801]
- Sessa L, et al. Noncoding RNA synthesis and loss of Polycomb group repression accompanies the colinear activation of the human HOXA cluster. *RNA.* 2007; 13:223–239. [PubMed: 17185360]
- Kashyap V, et al. Epigenomic reorganization of the clustered Hox genes in embryonic stem cells induced by retinoic acid. *J Biol Chem.* 2011; 286:3250–3260. [PubMed: 21087926]
- Novak P, et al. Epigenetic inactivation of the HOXA gene cluster in breast cancer. *Cancer Res.* 2006; 66:10664–10670. [PubMed: 17090521]
- Rauch T, et al. Homeobox gene methylation in lung cancer studied by genome-wide analysis with a microarray-based methylated CpG island recovery assay. *Proc Natl Acad Sci USA.* 2007; 104:5527–5532. [PubMed: 17369352]
- Laurent L, et al. Dynamic changes in the human methylome during differentiation. *Genome Res.* 2010; 20:320–331. [PubMed: 20133333]
- Musch T, Oz Y, Lyko F, Breiling A. Nucleoside drugs induce cellular differentiation by caspase-dependent degradation of stem cell factors. *PLoS One.* 2010; 5:e10726. [PubMed: 20502711]

15. Fouse SD, et al. Promoter CpG methylation contributes to ES cell gene regulation in parallel with Oct4/Nanog, PcG complex, and histone H3 K4/K27 trimethylation. *Cell Stem Cell*. 2008; 2:160–169. [PubMed: 18371437]
16. Wu SC, Zhang Y. Active DNA demethylation: many roads lead to Rome. *Nat Rev Mol Cell Biol*. 2010; 11:607–620. [PubMed: 20683471]
17. Ito S, et al. Tet proteins can convert 5-methylcytosine to 5-formylcytosine and 5-carboxylcytosine. *Science*. 2011; 333:1300–1303. [PubMed: 21778364]
18. He YF, et al. Tet-mediated formation of 5-carboxylcytosine and its excision by TDG in mammalian DNA. *Science*. 2011; 333:1303–1307. [PubMed: 21817016]
19. Ito S, et al. Role of Tet proteins in 5mC to 5hmC conversion, ES-cell self-renewal and inner cell mass specification. *Nature*. 2010; 466:1129–1133. [PubMed: 20639862]
20. Koh KP, et al. Tet1 and Tet2 regulate 5-hydroxymethylcytosine production and cell lineage specification in mouse embryonic stem cells. *Cell Stem Cell*. 2011; 8:200–213. [PubMed: 21295276]
21. Ficiz G, et al. Dynamic regulation of 5-hydroxymethylcytosine in mouse ES cells and during differentiation. *Nature*. 2011; 473:398–402. [PubMed: 21460836]
22. Wu H, et al. Genome-wide analysis of 5-hydroxymethylcytosine distribution reveals its dual function in transcriptional regulation in mouse embryonic stem cells. *Genes Dev*. 2011; 25:679–684. [PubMed: 21460036]
23. Pastor WA, et al. Genome-wide mapping of 5-hydroxymethylcytosine in embryonic stem cells. *Nature*. 2011; 473:394–397. [PubMed: 21552279]
24. Williams K, et al. TET1 and hydroxymethylcytosine in transcription and DNA methylation fidelity. *Nature*. 2011; 473:343–348. [PubMed: 21490601]
25. Xu Y, et al. Genome-wide regulation of 5hmC, 5mC, and gene expression by Tet1 hydroxylase in mouse embryonic stem cells. *Mol Cell*. 2011; 42:451–464. [PubMed: 21514197]
26. Kriaucionis S, Heintz N. The nuclear DNA base 5-hydroxymethylcytosine is present in Purkinje neurons and the brain. *Science*. 2009; 324:929–930. [PubMed: 19372393]
27. Globisch D, et al. Tissue distribution of 5-hydroxymethylcytosine and search for active demethylation intermediates. *PLoS One*. 2010; 5:e15367. [PubMed: 21203455]
28. Haffner MC, et al. Global 5-hydroxymethylcytosine content is significantly reduced in tissue stem/progenitor cell compartments and in human cancers. *Oncotarget*. 2011; 2:627–637. [PubMed: 21896958]
29. Langemeijer SM, et al. Acquired mutations in TET2 are common in myelodysplastic syndromes. *Nat Genet*. 2009; 41:838–842. [PubMed: 19483684]
30. Tefferi A, et al. Detection of mutant TET2 in myeloid malignancies other than myeloproliferative neoplasms: CMML, MDS, MDS/MPN and AML. *Leukemia*. 2009; 23:1343–1345. [PubMed: 19295549]
31. Andrews PW. From teratocarcinomas to embryonic stem cells. *Philos Trans R Soc Lond B Biol Sci*. 2002; 357:405–417. [PubMed: 12028783]
32. Pal R, Ravindran G. Assessment of pluripotency and multilineage differentiation potential of NTERA-2 cells as a model for studying human embryonic stem cells. *Cell Prolif*. 2006; 39:585–598. [PubMed: 17109641]
33. Sandoval J, et al. Validation of a DNA methylation microarray for 450,000 CpG sites in the human genome. *Epigenetics*. 2011; 6:692–702. [PubMed: 21593595]
34. Lister R, et al. Human DNA methylomes at base resolution show widespread epigenomic differences. *Nature*. 2009; 462:315–322. [PubMed: 19829295]
35. Meissner A, et al. Genome-scale DNA methylation maps of pluripotent and differentiated cells. *Nature*. 2008; 454:766–770. [PubMed: 18600261]
36. Irizarry RA, et al. The human colon cancer methylome shows similar hypo- and hypermethylation at conserved tissue-specific CpG island shores. *Nat Genet*. 2009; 41:178–186. [PubMed: 19151715]
37. Boyer LA, et al. Core transcriptional regulatory circuitry in human embryonic stem cells. *Cell*. 2005; 122:947–956. [PubMed: 16153702]

38. Huang Y, et al. The behaviour of 5-hydroxymethylcytosine in bisulfite sequencing. *PLoS One*. 2010; 5:e8888. [PubMed: 20126651]
39. Li Z, et al. Deletion of Tet2 in mice leads to dysregulated hematopoietic stem cells and subsequent development of myeloid malignancies. *Blood*. 2011; 118:4509–4518. [PubMed: 21803851]
40. Ko M, et al. Ten-Eleven-Translocation 2 (TET2) negatively regulates homeostasis and differentiation of hematopoietic stem cells in mice. *Proc Natl Acad Sci USA*. 2011; 108:14566–14571. [PubMed: 21873190]
41. Pronier E, et al. Inhibition of TET2-mediated conversion of 5-methylcytosine to 5-hydroxymethylcytosine disturbs erythroid and granulomonocytic differentiation of human hematopoietic progenitors. *Blood*. 2011; 118:2551–2555. [PubMed: 21734233]
42. Quivoron C, et al. TET2 inactivation results in pleiotropic hematopoietic abnormalities in mouse and is a recurrent event during human lymphomagenesis. *Cancer Cell*. 2011; 20:25–38. [PubMed: 21723201]
43. Gudas LJ, Wagner JA. Retinoids regulate stem cell differentiation. *J Cell Physiol*. 2011; 226:322–330. [PubMed: 20836077]
44. Ferraiuolo MA, et al. The three-dimensional architecture of Hox cluster silencing. *Nucleic Acids Res*. 2010; 38:7472–7484. [PubMed: 20660483]
45. Kim YJ, Cecchini KR, Kim TH. Conserved, developmentally regulated mechanism couples chromosomal looping and heterochromatin barrier activity at the homeobox gene A locus. *Proc Natl Acad Sci USA*. 2011; 108:7391–7396. [PubMed: 21502535]
46. Noordermeer D, et al. The dynamic architecture of Hox gene clusters. *Science*. 2011; 334:222–225. [PubMed: 21998387]
47. Valinluck V, Sowers LC. Endogenous cytosine damage products alter the site selectivity of human DNA maintenance methyltransferase DNMT1. *Cancer Res*. 2007; 67:946–950. [PubMed: 17283125]
48. Valinluck V, et al. Oxidative damage to methyl-CpG sequences inhibits the binding of the methyl-CpG binding domain (MBD) of methyl-CpG binding protein 2 (MeCP2). *Nucleic Acids Res*. 2004; 32:4100–4108. [PubMed: 15302911]
49. Yildirim O, et al. Mbd3/NURD Complex Regulates Expression of 5-Hydroxymethylcytosine Marked Genes in Embryonic Stem Cells. *Cell*. 2011; 147:1498–1510. [PubMed: 22196727]
50. Nestor CE, et al. Tissue type is a major modifier of the 5-hydroxymethylcytosine content of human genes. *Genome Res*. 2012; 22:467–477. [PubMed: 22106369]
51. Groninger E, et al. Aging and chronic sun exposure cause distinct epigenetic changes in human skin. *PLoS Genet*. 2010; 6:e1000971. [PubMed: 20523906]
52. Mohn F, Weber M, Schübeler D, Roloff TC. Methylated DNA immunoprecipitation (MeDIP). *Methods Mol Biol*. 2009; 507:55–64. [PubMed: 18987806]
53. Ossowski S, et al. Sequencing of natural strains of *Arabidopsis thaliana* with short reads. *Genome Res*. 2008; 18:2024–2033. [PubMed: 18818371]
54. Langmead B, Trapnell C, Pop M, Salzberg SL. Ultrafast and memory-efficient alignment of short DNA sequences to the human genome. *Genome Biol*. 2009; 10:R25. [PubMed: 19261174]
55. Dreszer TR, et al. The UCSC Genome Browser database: extensions and updates. *Nucleic Acids Res*. 2012; 40 (database issue):D918–23. [PubMed: 22086951]

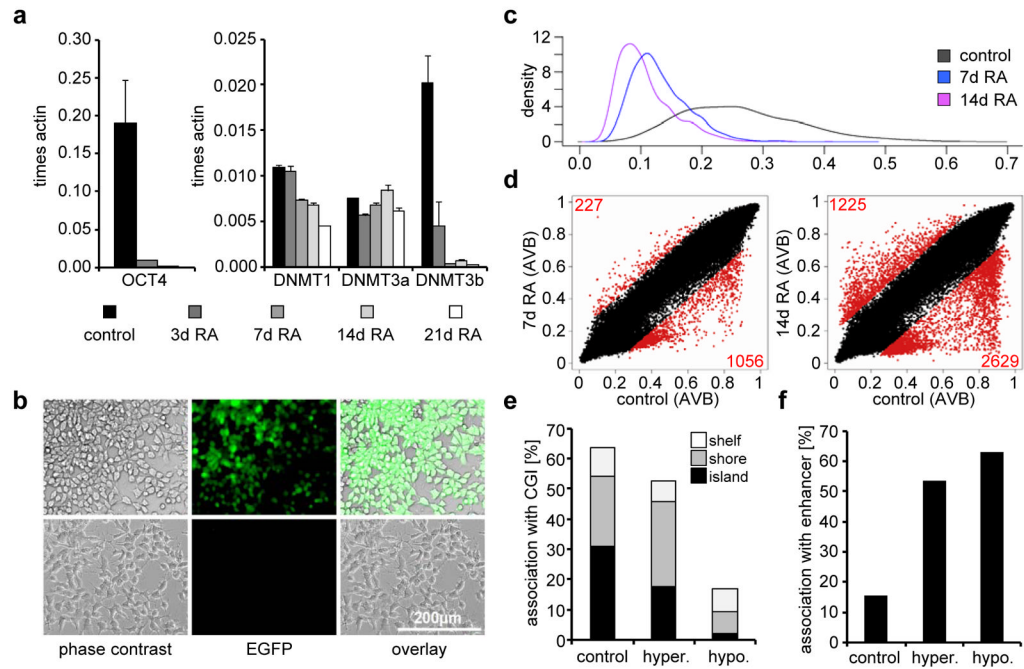


Figure 1. Pluripotency features and DNA methylation profiles of NT2 cells upon retinoic acid induction

(a) Expression of *OCT4*, *DNMT1*, *DNMT3a* and *DNMT3b* in untreated NT2 cells and cells treated for 3, 7, 14 and 21 days with retinoic acid (RA). qRT-PCR measurements with at least three biological replicates were internally normalised to the corresponding β -actin expression levels. Standard deviations are indicated by error bars. (b) Microscopic images of NT2 cells showing the expression of EGFP under the control of the *OCT4*-promoter (first row) and the same cells after treatment with retinoic acid for 7 days (second row). The first column shows the light microscopic images (phase contrast), the second column EGFP fluorescence, the third column an overlay. (c) Density plot showing the distribution of the AVB-values (x-axis) of 3091 non-CpG methylation states interrogated by the Infinium450K BeadChip, measured in uninduced NT2 cells (black, mean = 0.27) and cells treated for 7 days (blue, mean = 0.13) and 14 days (purple, mean = 0.11) with RA. (d) Scatter plots showing the comparison of Illumina DNA methylation profiles (including non-CpG sites) of untreated NT2 cells with profiles of cells treated for 7 days (left plot) and 14 days (right plot) with RA. Red dots and numbers indicate differentially methylated sites. (e) Bar diagram showing the association of all sites interrogated by the Infinium450K BeadChip (control), RA-induced hypomethylated sites (hypo.) and hypermethylated sites (hyper.) with CpG islands, shelf and shore regions. (f) Bar diagram showing the correlation of RA-induced differentially methylated sites (hypo- or hypermethylated compared to controls) identified using the Infinium450K BeadChip with annotated enhancer regions.

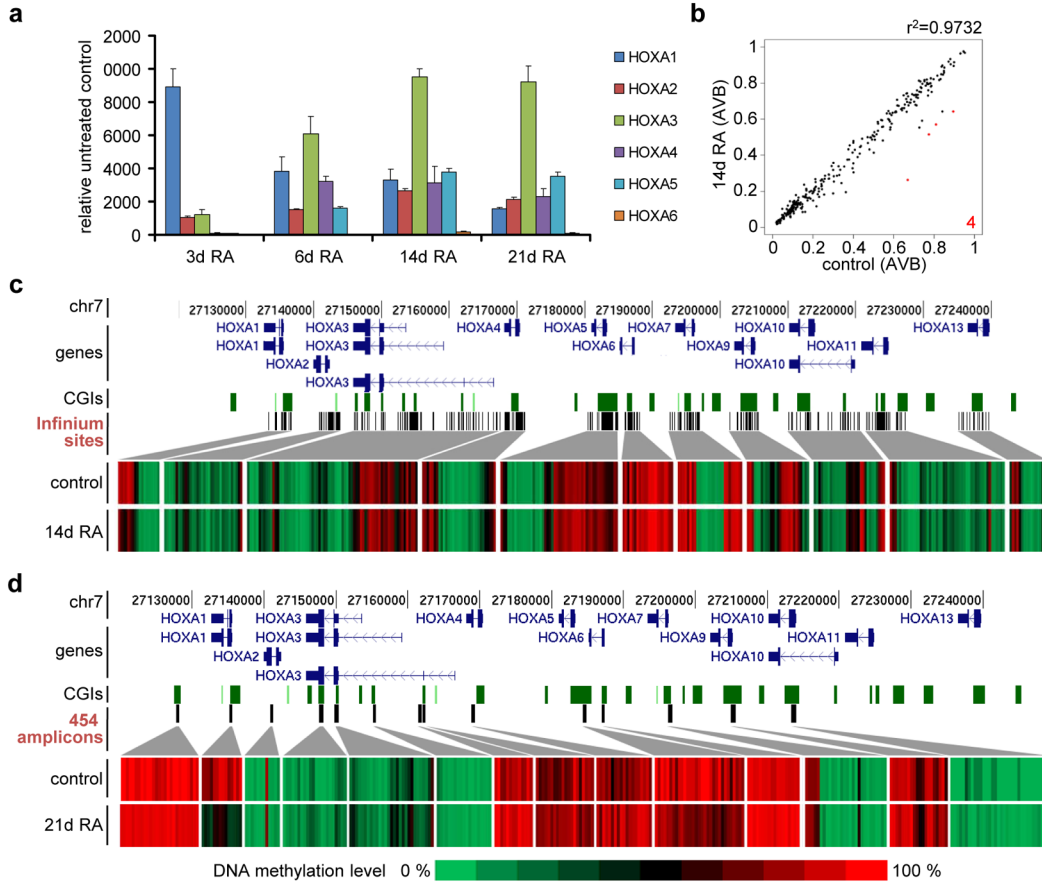


Figure 2. Epigenetic regulation of the *HOXA* cluster

(a) qRT-PCR expression analysis of *HOXA* genes (1 to 6) after RA treatment for 3, 6, 14 and 21 days. qPCR values were internally normalised to the corresponding *lamin-b* and β -*actin* expression levels. Expression values indicate fold induction compared to the non-treated control. All treatments and measurements were repeated three times. Standard deviations are indicated by error bars. (b) Scatter plot showing the comparison of Illumina DNA methylation values of sites located within the *HOXA* cluster of NT2 cells treated for 14 days with RA with those of untreated cells. Red dots indicate differentially methylated sites. Only four sites were significantly hypomethylated upon RA treatment, corresponding to the *HOXA1* gene body. (c) Array-predicted DNA methylation levels in the *HOXA* cluster in untreated NT2 cells (control) and cells treated for 14 days with retinoic acid (14d RA). *HOXA* transcription units on chromosome 7 are indicated in dark blue, CpG islands as green squares and interrogated Infinium sites as black bars. Genomic features are viewed as custom tracks in the UCSC genome browser⁵⁵. (d) DNA methylation levels in the *HOXA* cluster, as obtained by 454 bisulfite sequencing of selected amplicons (black bars) in untreated NT2 cells (control) and in cells treated for 21 days with retinoic acid (21d RA). *HOXA* transcription units on chromosome 7 (in dark blue), CGIs (green bars) and 454 amplicons (black bars) are indicated. Genomic features are viewed as custom tracks in the UCSC genome browser⁵⁵.

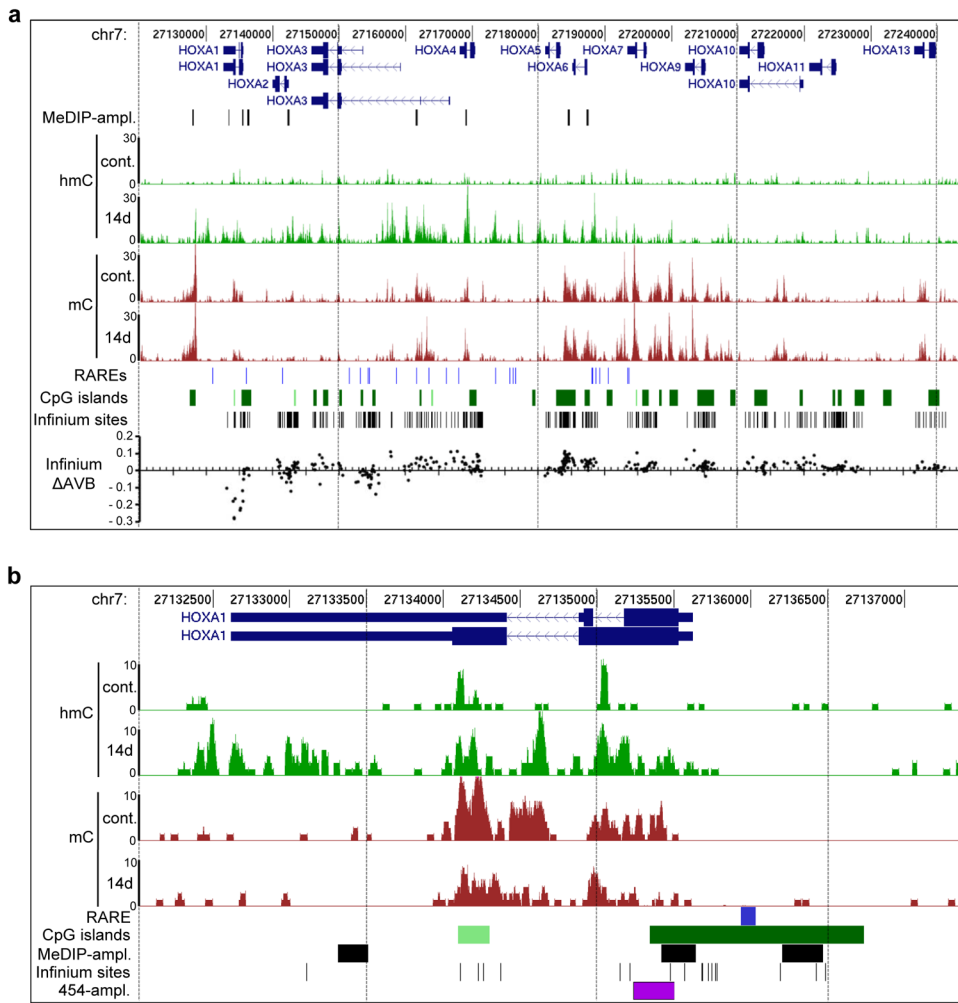


Figure 3. Distribution of 5mC and 5hmC within the *HOXA* cluster

(a) hMeDIP-seq (hmC) and MeDIP-seq (mC) profiles of the *HOXA* cluster in untreated NT2 cells (cont.) and cells treated for 14 days with retinoic acid (14d). Enrichments are indicated as increase in the sequence coverage. *HOXA* transcription units on chromosome 7 are indicated on top in dark blue, below (h)MeDIP-amplicons are indicated as black lines. Potential retinoic acid response elements (RAREs)⁹ are shown as light blue lines below the profiles, CpG islands as green squares and sites interrogated by the Infinium450K BeadChip as black bars. At the bottom the difference of methylation values of the Infinium analysis (Δ AVB) between untreated and NT2 cells treated for 14 days with RA for each Infinium site is indicated. Genomic features are viewed as custom tracks in the UCSC genome browser⁵⁵ (b) Detailed hMeDIP-seq (hmC) and MeDIP-seq (mC) profiles at the *HOXA1* locus in untreated NT2 cells (cont.) and cells treated for 14 days with retinoic acid (14d). The *HOXA1* RARE (blue bar), CpG islands (green squares), (h)MeDIP-amplicons (black squares), Infinium sites (black lines) and the 454 bisulfite sequencing amplicon (purple square) are indicated below the profiles. Genomic features are viewed as custom tracks in the UCSC genome browser⁵⁵.

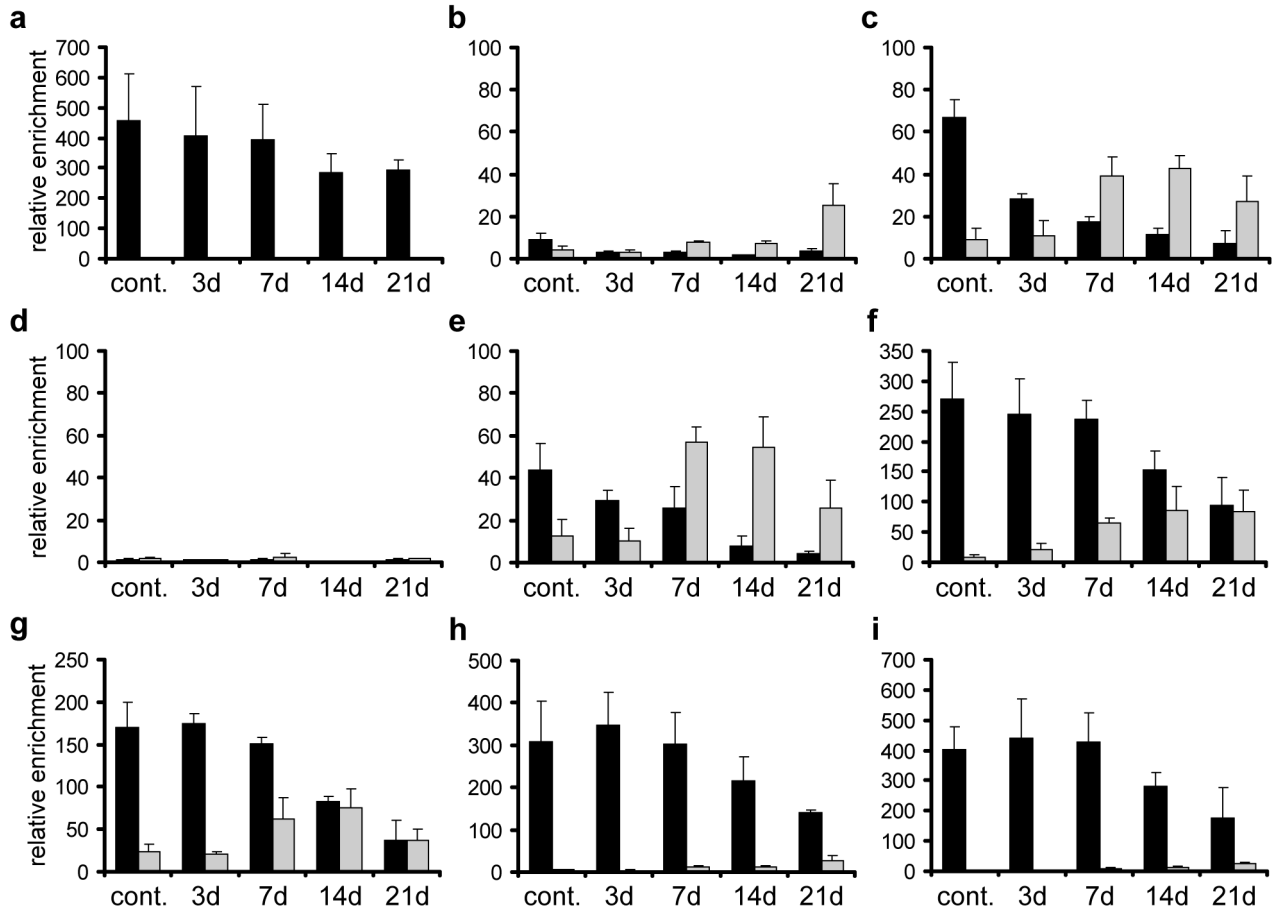


Figure 4. Levels of 5mC and 5hmC at selected regions of the *HOXA* cluster

Genomic DNA from untreated NT2 cells and cells treated for 3, 7, 14 and 21 days with retinoic acid was analysed by (h)MeDIP using antibodies against 5mC and 5hmC. Immunoprecipitated DNA was amplified by gene specific qPCR. The following regions were analysed: (a) *HOXA1* downstream CpG island, (b) *HOXA1* second exon (covering a potential NANOG/OCT4 binding site³⁷), (c) *HOXA1* promoter/1st exon, (d) *HOXA1* upstream RARE (e) *HOXA2* promoter/1st exon (f) *HOXA3* 2nd CpG island (g) *HOXA4* 2nd exon (h) *HOXA5-6* intergenic CpG island (i) *HOXA6* promoter/1st exon. Enrichments were calculated relative to the unmethylated *UEB2* control. 5mC values are shown as black bars, 5hmC values as grey bars. Diagrams show the results of at least three independent experiments. Standard deviations are indicated by error bars.

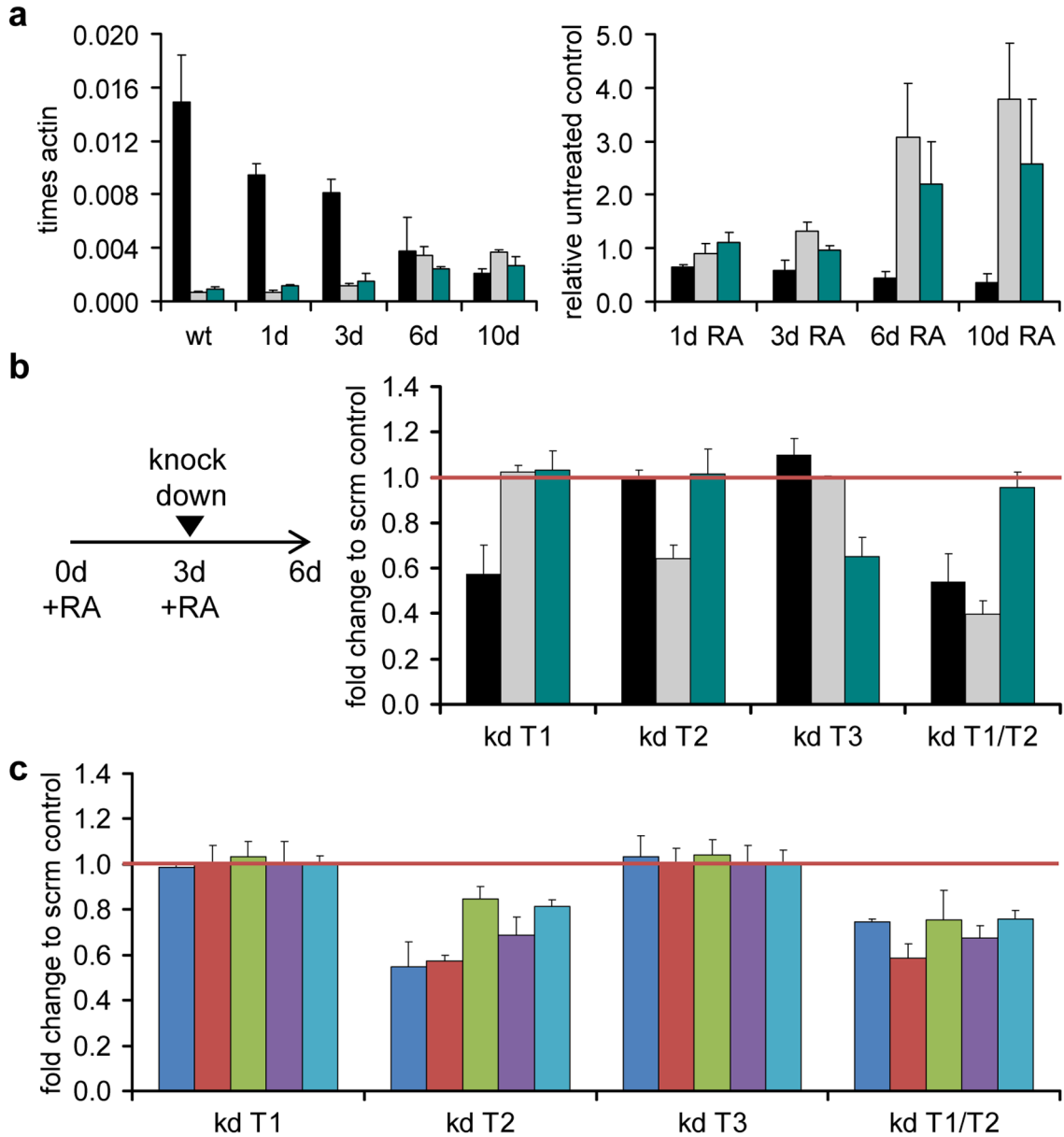


Figure 5. TET2 is necessary for the maintenance of HOXA activity

(a) qRT-PCR expression analysis of the three *TET* genes after RA treatment for 1, 3, 6 and 10 days. The left panel shows the expression levels of *TET1* (black bars), *TET2* (grey bars) and *TET3* (green bars) as a fraction of the β -actin expression levels. The right panel shows the expression changes of the three *TET* mRNAs during RA treatment relative to the untreated control, internally normalised to the corresponding expression levels of *lamin-b* and β -actin. (b) qRT-PCR expression analysis of *TET1* (black bars), *TET2* (grey bars) and *TET3* (green bars) after RA treatment and successive depletion with specific siRNA pools in single knock downs (kd T1, kd T2, kd T3) or in a TET1/TET2 double knock down (kd T1/T2). NT2 cells were treated for 3 days with retinoic acid, replated and transfected with siRNAs. After 3 more days cells were harvested and total RNA for qRT-PCR analysis was isolated. Y-axis values indicate fold change compared to the scrambled knock down control (non-targeting pool). qPCR values were internally normalised to the corresponding *lamin-b*

and β -actin expression levels. (c) qRT-PCR expression analysis of *HOXA1* (blue bars), *HOXA2* (red bars), *HOXA3* (green bars), *HOXA4* (purple bars), *HOXA5* (light blue bars) after RA treatment and successive TET-depletion with specific siRNAs in single knock downs (kd T1, kd T2, kd T3) or in TET1/TET2 double combination (kd T1/T2). Y-axis values indicate fold change compared to the scrambled knock down control (non-targeting pool). qPCR values were internally normalised to the corresponding *lamin-b* and β -actin expression levels.

Treatments and measurements in (a)–(c) were repeated at least three times. Standard deviations are indicated by error bars.

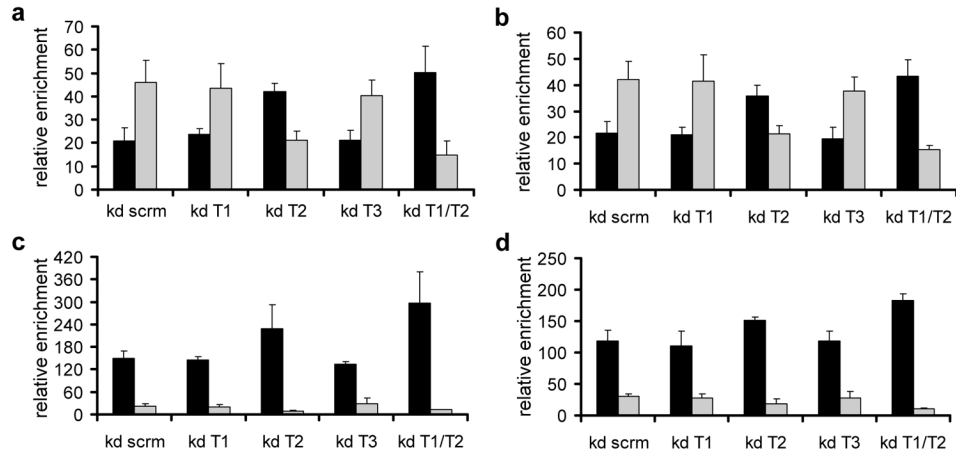


Figure 6. TET2 is mainly responsible for the 5mC-5hmC conversion in the *HOXA* cluster during retinoic acid induction

The diagrams show the distribution of 5mC and 5hmC at four regions of the *HOXA* cluster in NT2 cells transfected with control siRNAs (non-targeting pool - kd scrn), siRNA pools against TET1 (kd T1), TET2 (kd T2), TET3 (kd T3) and TET1/TET2 (kd T1/T2). NT2 cells were treated for 3 days with retinoic acid, replated and transfected with siRNAs. After 3 additional days, cells were harvested and genomic DNA for (h)MeDIP analysis with antibodies specific for 5mC and 5hmC was isolated. Immunoprecipitated DNA was amplified by gene specific qPCR. The following regions were analysed: (a) *HOXA1* promoter/1st exon, (b) *HOXA2* promoter/1st exon, (c) *HOXA3* 2nd CpG island and (d) *HOXA4* 2nd exon. Enrichments were calculated relative to the unmethylated *UEB2* control. 5mC values are shown as black bars, 5hmC values as grey bars. Diagrams show the results of three independent experiments. Standard deviations are indicated by error bars.

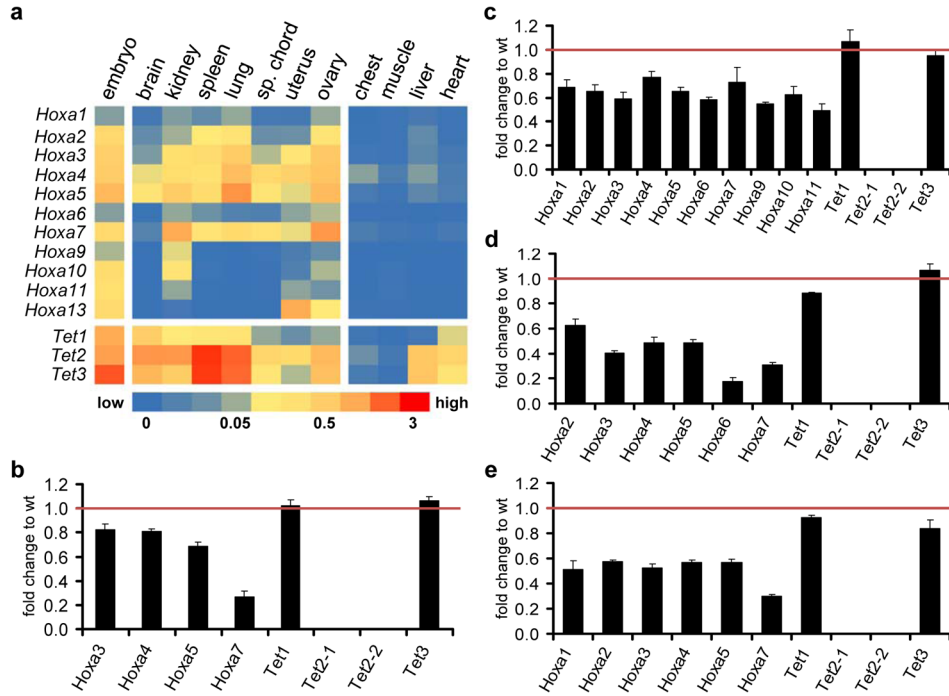


Figure 7. Expression of *Hoxa* genes is reduced in mouse *Tet2*^{-/-} tissues

(a) qRT-PCR expression analysis of the eleven *Hoxa* and three *Tet* genes in murine wild type tissues (indicated above the columns). The heat map shows average *Hoxa* and *Tet* expression as percentage of the internal *GPDH* levels. Expression patterns of both groups of genes in 13.5 days wild type embryos is shown as a positive control (most left column). Four examples of tissues with very low or absent expression are also shown (chest, muscle, liver, heart). (b)–(d) qRT-PCR expression analysis of *Hoxa* genes that showed significant levels in (a) and the three *Tet* genes in selected *Tet2*^{-/-} tissues. Diagrams show the expression as fold change relative to the wild type (=1). For *Tet2*, two different primer pairs were used³⁹. (b) brain, (c) kidney, (d) spleen, (e) lung. Standard deviations of three replicates are indicated by error bars.

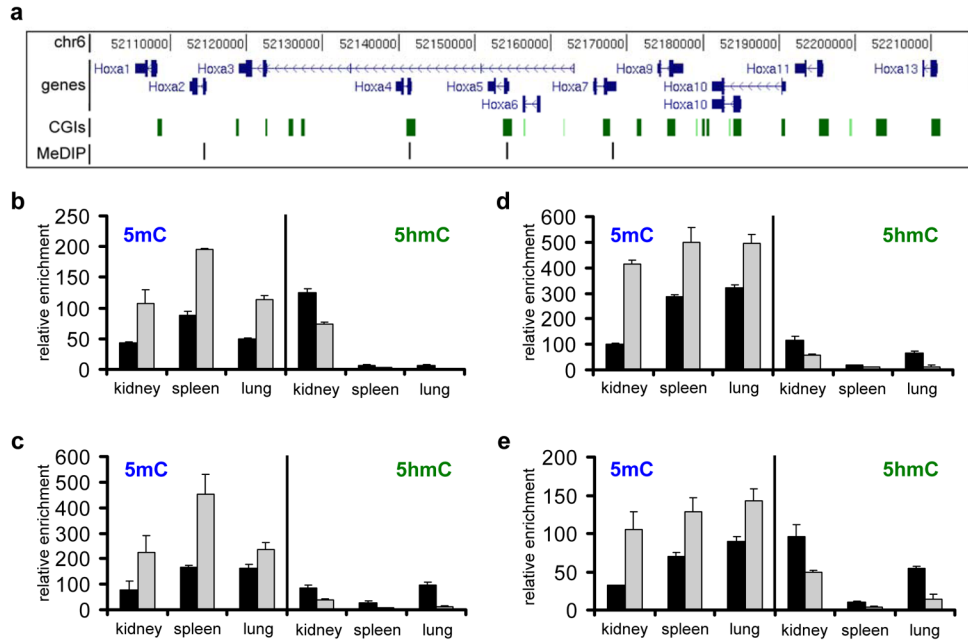


Figure 8. Levels of 5mC and 5hmC at selected regions of the murine *Hoxa* cluster in control and *Tet2*^{-/-} tissues

Genomic DNA was isolated from three tissues showing significant *Hoxa* expression in the wild type situation (kidney, spleen and lung) and used for (h)MeDIP analysis with antibodies specific for 5mC and 5hmC. (a) Diagram showing the mouse *Hoxa* transcription units on chromosome 6 (in dark blue), the CpG islands within the cluster (green squares) and the four (h)MeDIP-amplicons (indicated as black lines) used for the analysis. Genomic features are viewed as custom tracks in the UCSC genome browser⁵⁵. The following regions were analysed: (b) *mHoxa2* promoter, (c) *mHoxa4* 1st exon, (d) *mHoxa5* 1st exon and (e) *mHoxa7* promoter. The diagrams show the distribution of 5mC (left in each panel) and 5hmC (right in each panel) at four regions of the mouse *Hoxa* cluster in three tissues (kidney, spleen, lung) in wt (black bars) and *Tet2*^{-/-} (grey bars). Enrichments were calculated relative to the unmethylated *mGapdh* and *mbeta-actin* controls. Standard deviations of three replicates are indicated by error bars.